Transforming and validating urban microclimate data with multi-sourced microclimate datasets for building energy modelling at urban scale

Yi Yang[a], Qili Gu[a], Hailu Wei[a], Hua Liu[b], Wei Wang[a, 1], Shen Wei[c, 2]

[a] *School of Architecture, Southeast University, Nanjing, Jiangsu Province, China, 210096*

[b] *Architecture and Engineering Co., Ltd. of Southeast University, Nanjing, Jiangsu Province, China, 210096*

[c] *The Bartlett School of Sustainable Construction, University College London (UCL), 1-19 Torrington Place, London WC1E 7HB, United Kingdom*

Abstract: Weather data is one of the most important inputs for a reliable building energy simulation, and in current studies, EnergyPlus Weather (EPW), historically measured by a few suburban weather stations, is most widely used. Weather, however, is shaped by urban morphology and other factors, and therefore transforming weather files using tools like urban weather generator into urban area becomes necessary. This study investigated the differences between multi-sourced weather datasets after transforming, and in turn the impact on urban building energy simulation. One campus block was selected as a case study, with forty-one urban blocks obtained along with their urban morphologies. One microclimate station and sixteen sensors were installed to collect weather data to validate multi-sourced weather files for energy simulation models. The study results showed the root mean square error (RMSE) of temperature differences between suburban weather station, EPW and microclimate station on campus was 2.1°C and 4.3°C, respectively, turned into 1.2°C and 4.1°C, respectively after transforming. With respect to building energy use, the mean absolute percentage difference (MAPD) of cooling-energy use intensity between the ones calculated from the above mentioned three datasets was 32.4% and 13.1%, respectively, turned into 25.8% and 4.1%, respectively after transforming. Meanwhile, the MAPD of heating-energy use intensity was 27.2% and 116.3%, respectively, turned into 12.7% and 93.6%, respectively after transforming. This study provides references of selecting weather data for urban building energy modelling to achieve more reliable energy decision-making process.

Keywords: Urban Building Energy Modelling; Urban Microclimate; Microclimate

---

[1] Wei Wang, Associate Professor, weiwang@seu.edu.cn

[2] Shen Wei, Associate Professor, shen.wei@ucl.ac.uk

transforming; Multi-sourced validation

1. Introduction

Until 2022, the urbanization rate in China has reached 65.22% [1]. This urban sprawl has produced profound changes in the urban physical environment, consequently increasing urban energy consumption and global carbon emissions [2,3]. As known, buildings are responsible for one-third of energy consumption in cities [4], and there exists a great and untapped opportunity to create and transform urban buildings to more sustainable and energy-efficient environment in city context [5]. In this way, Urban Building Energy Modelling (UBEM), that was developed from Building Energy Modelling (BEM), has been developed to combine various urban data with energy simulation tools [6,7]. Subsequently, efficient UBEM frameworks like City Building Energy Saver (CityBES) [8], UBEM.io [9], City Energy Analyst (CEA) [10], and so on, were proposed can predict building energy demand at larger and broader spatial levels.

In those existing UBEM frameworks, weather data has been recognized as an essential input parameter [11–13]. While modelling energy demand of buildings, major climatic parameters as the important influencing factors include outdoor temperature, relative humidity, wind, and solar radiation [14], which can be generated as a weather file, named as EnergyPlus weather (EPW) in building simulation tools. Current default EPW file used in UBEM are usually Typical Meteorological Year (TMY), and it was mainly derived from a long period of historical weather records with averaged annual hourly meteorological data [15,16]. The inherent nature of TMY excluding extreme weather and weather changes makes them less suitable for investigating the effect of potential local microclimate on building energy performance as microclimate usually deviates significantly from TMYs [17].

An alternative to obtain weather data is using weather stations located in suburb areas, which is relatively more accurate than TMY. In this approach, at least one-year period of urban weather dataset should be collected to generate the EPW file with the tools, e.g., pyepw or Elements. However, in central urban areas, the urban microclimate may be quite different from rural climate due to both the form and the fabric of urban landscape [18]. At a larger spatial level such as a neighborhood or even a city, the concentration of human activities and man-made buildings will further contribute to changes in the inthernal microclimate of the city. A typical example of this effect is Urban Heat Island (UHI), which results in higher temperature in urban areas than in rural areas [19]. Guattari et al. [20] simulated the energy consumption of individual buildings based on meteorological data collected for the central city and suburban areas of Rome to assess the impact of different climate boundaries on building energy performance. The results showed that the average building cooling demand increased by about 30% and the average heating demand decreased by about 11%. Hong et al. [21] simulated the annual cooling and heating demand of a typical building using data from 27 meteorological sites in San Francisco, and the results varied by 100% and 65%, respectively, and the peak electricity demand reached a 30% difference. Therefore, to accurately simulate building energy demand at urban level, it is important to consider the impact of urban microclimate [22,23].

The current methods used to obtain urban microclimate data can be divided into three categories [24]. Field measurement is the earliest method, and it uses monitoring instruments to measure climate parameters in a specific geographic location [25,26], which is labor-intensive and costly. The second method uses remote sensing and GIS tools to invert the environmental conditions near the ground through data obtained from remote sensors or satellites [27–29]. Such method, however, is impossible to form continuous urban weather files since satellite photos are taken periodically. The third method is to simulate/calcualte microclimate, and this method can facilitate the flexible weather data both spatially and temporally by transforming computational models [30,31]. To simulate/calcualte urban microclimate data, there are three types of computational models, namely, numerical weather prediction model, Computational Fluid Dynamics (CFD) model, and Urban Canopy Model (UCM). In the first model, long-term historical microclimate data may be essential for a basic energy simulation run, and prediction techniques assisted with numerical models, such as machine learning [32] and large eddy simulation [33], can be applied to forecast a complete weather file within a few meters horizontally, and then resolve micro-climate features at neighborhood scale. In another two models, urban morphology is an essential component and has an impact in turn on urban microclimate and energy consumption [34].

Urban morphology consists of both physical form of buildings, urban blue-green space, and so on, and those have a positive effect on reducing UHI effect and for an exact urban block, its specific morphology can form its own microclimate [35]. Therefore, simulating buildings' energy demand of an exact location in urban context requires its typical meteorological data for a customized weather [36]. Long (longer than one year) and accurate field data measured from exact locations, however, is quite difficult to obtain. To overcome this issue, Urban Weather Generator (UWG), as a typical UCM model, was developed by Bueno et al. [37], and it can generate a new weather file for an exact location through transforming the rural or TMY weather files by considering the impact of urban morphology on the urban microclimate variables for a given neighborhood. Subsequently, researchers further enriched the UWG by introducing relevant urban morphology of a block into its microclimate and energy analysis [38]. For example, Detommaso et al. [39] have input the UWG-processed weather files to ENVI-met, and this approach has been proven to provide sufficiently reliable data for simulating microclimate. To improve the accuracy of energy simulation, Kamal et al. [40] have applied UWG to transform raw weather data with urban morphological parameters, and Ma et al. [41] have applied UWG to transform the TMY file to an urban block, by integrating morphological parameters for localized microclimate estimation, and further simulated the multi-scale building energy. However, the accuracy prediction of building energy performance metrics using detailed BEM software, like EnergyPlus, in urban areas for the transformed microclimate data is still lacking, and the rural or TMY weather data always cannot reflect the actual situation. Oller et al. [42] pointed out that since the lack of precise meteorological data in exact locations, data from suburban weather stations is generally used, with lack of information indicating the potential errors resulted in the simulated performance of buildings.

Many studies have confirmed that there are differences between building energy simulation results due to using weather data from different sources. Although these differences can be reduced by transforming the weather files, a comprehensive understanding on the effects from all possible sources of weather data is still missing, as well as their contributions to the simulated energy consumption at urban levels. To fill this research gap, this study selected multi-sourced weather files and combined them with UWG to obtain transformed weather data, integrating with EnergyPlus to simulate building energy consumption in the study area under all weather files. A comparative analysis of the data was used to derive error ranges in weather variables and differences ranges between the energy simulation results calculated using multi-sourced weather files and those obtained using field measured weather files. Based on the comparison results, a reference for the priority of weather data selection in subsequent urban building energy modelling studies can be provided.

2. Methodology

2.1 Comparison workflow

This study created the UBEM of urban blocks with building geometries and properties, and used EnergyPlus to simulate building energy demand. Figure 1 shows the overall workflow of this study, which consists of four major steps:

- Step 1 (Weather Data Collection): in this step, the weather data were obtained from multiple sources, including typical EPW file from EnergyPlus website, the weather station of Nanjing city, one long-term microclimate station and sixteen stationary sensors in the case study campus.

- Step 2 (Physical Modeling): in this step, forty-one different blocks with different urban morphologies were randomly generated. Geometric characteristics (e.g., building height, building density, building floor area and window-to-wall ratio), and non-geometric characteristics (e.g., heating, ventilation, air conditioning system, heat transfer of building envelopes and occupant behavior) of the buildings were obtained from on-site survey and national reference standards, and then the building energy models were created according to these data.

- Step 3 (Weather Data Processing): in this step, the UWG was applied to transform weather data for each block according to its morphology, with a total of five comparisons carried out to identify the differences between multi-sourced weather files.

- Step 4 (Energy Simulation): in this step, comparison of model estimates of building energy consumption using EnergyPlus as being forced with weather files using two alternative methods was carried out using mean absolute percentage difference (MAPD).

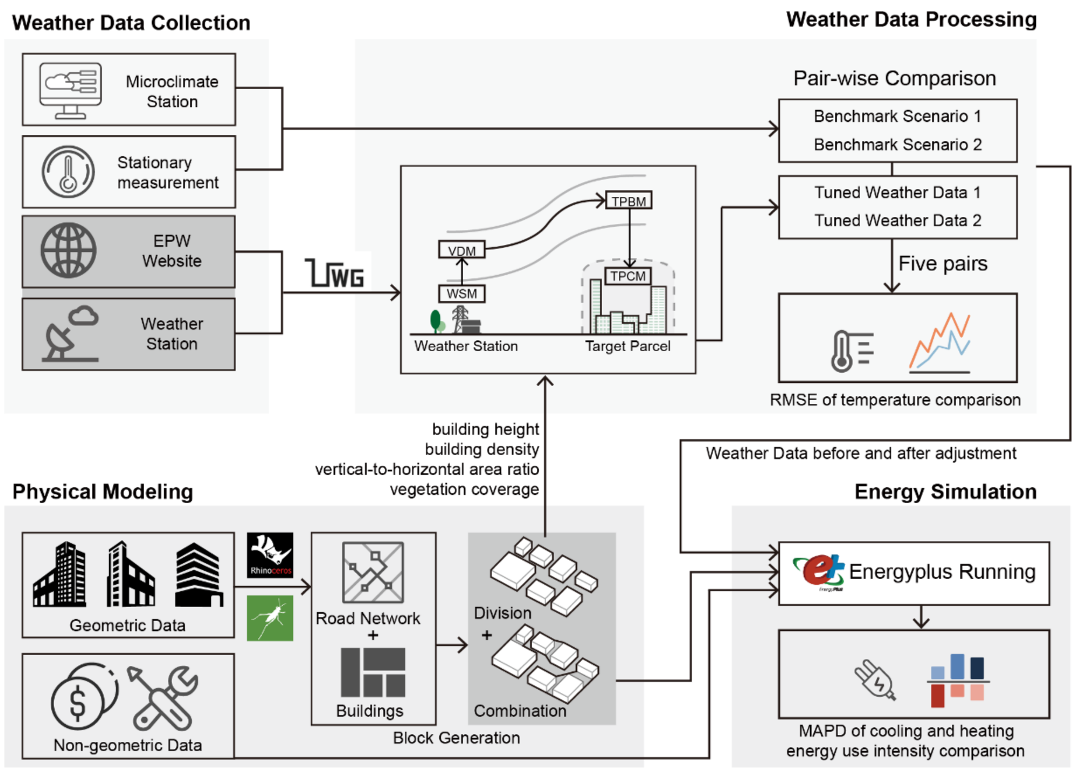

Figure 1: Workflow of multi-sourced weather comparison in UBEM process

2.2 Case study urban area

This study has selected the Sipailou campus of Southeast University (SEU) (Figure 2) as a case study. This university campus is located in the central area of Nanjing, Jiangsu Province, China. It has a total area of 411,309m^2 and this size is an appropriate scale for neighborhood level analysis. There are thirty-eight buildings on the campus with various functions, such as office building, laboratory buildings, teaching buildings and multi-use buildings. Multi-use buildings may include classrooms, offices for both research students and academic staff, research laboratories, etc. The buildings on the campus have floors between 1 and 15, with an average of 5 floors. As a typical university campus in China, the buildings were mainly made of brick-concrete and reinforced concrete structures.

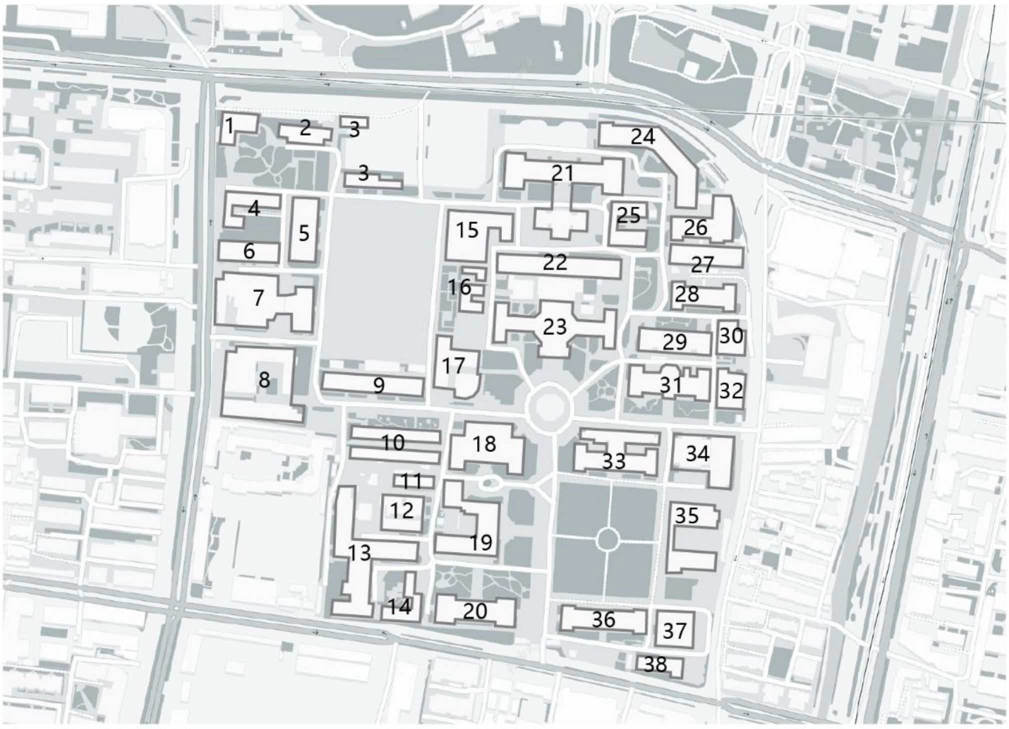

Figure 2: The case study campus

2.3 Multi-sourced microclimate data

In this study, the raw weather data were obtained from four different sources, namely EnergyPlus weather file (EPW), data from the Nanjing weather station (WS), data from the microclimate station in SEU (SEU) and data from stationary distributed microclimate experiments (Si). The specific methods used to obtain these weather data and the weather information they contain were described below.

The EPW weather file for Nanjing was downloaded from the EnergyPlus weather website [43]. The data for cities in China comes from the China Standard Weather Data (CSWD), which is a specific meteorological dataset for building thermal analysis, with data measured between 1971 and 2003 from 270 meteorological stations in China. The climatic parameters used in this study included air temperature, relative humidity, direct solar radiation, wind speed and wind direction, which are commonly adopted in existing studies [44].

The local climatic data of Nanjing was obtained from the Nanjing weather station (District Station No. 58238), which is 53.8 km away from the case study campus. The data include hourly-measured air temperature, relative humidity, solar radiation, wind speed and wind direction, which were collected in 2020.

A local microclimate weather station has been installed under manufacturers' guidelines on the roof of a six-story building in SEU, since 2016, as shown in Figure 3. The location was selected with a consideration of potential shading from surrounding buildings or trees. The weather station measures air temperature, relative humidity, direct normal solar radiation, wind speed and wind direction, which are accessible from either a local storage via a Wifi channel or an online server. Table 1 has listed some major technical specifications about the measurements from this local weather station. The data used in this study was collected in 2020.

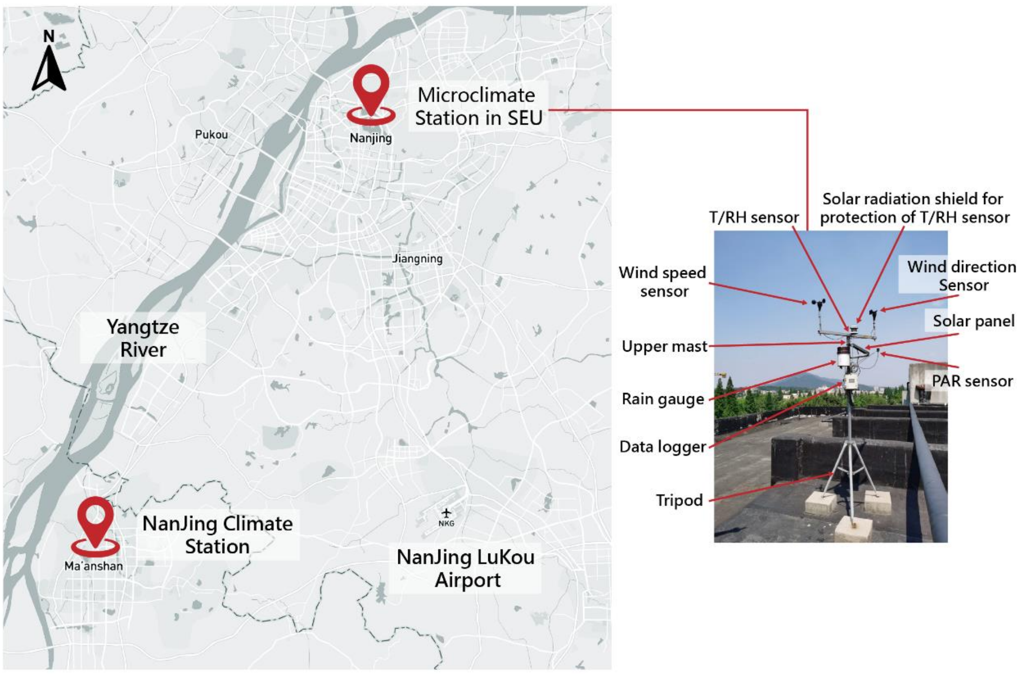

Figure 3: The local microclimate station on the campus

Table 1: Main technical specifications for the local microclimate station on the campus

	Data logger	Temperature /Humidity	Wind speed	Wind Direction	Solar radiation
Version	RX3003	S-THB-M002	S-WSB-M003	S-WDB-M003	S-LIB-M003
Operating temperature	-40~+60°C	-40~+75°C	-40~+75°C	-40~+70°C	-40~+75°C
Accuracy	-	T: ±0.21°C RH: ±2.5%	±1.1m/s or ±4%	±5°	±10 W/m^2 or ±5%
Resolution	-	T: 0.02°C RH: 0.1%	0.5 m/s	1.4°	1.25 W/m^2
Measurement range	-	T: -40~+75°C RH: 0~100%	0~76 m/s	0~355°	0~1280 W/m^2

To obtain more specific climatic conditions of different exact locations, besides the above local weather station, other sixteen stationary distributed measurement points were installed on the campus as well, with the locations indicated in Figure 4. Those sensors are installed at a height of 1m on the campus. The data from these points were collected to validate the weather file transformed by UWG for each block. These sensors measure air temperature, relative humidity, light intensity, CO_2 concentration and TVOC concentration. Among those parameters, temperature was selected for the validation, and regarding weather monitoring, DHT22 excels in precision as a humidity and temperature sensor with an accuracy of ±2% for relative humidity and accuracy of ±0.5°C for temperature [45]. Because the battery of sensors can only support 3 days, each time in close to 3 days, they need to be replaced manually. To avoid time-consuming and labor intensive, a duration of one-month monitoring was obtained and the data was collected in December, 2020. During validation, this study compared the one-month weather file transformed by UWG (that is December) with data from stationary distributed measurement points.

Figure 4: Stationary distributed measurement points on campus

2.4 Microclimate transforming and energy simulation

2.4.1 Urban block generation

In this part, the blocks used in the subsequent UWG model were generated. In order to divide the study area into separate blocks accurately, this study required information on building footprints, road networks and greenery, which can be obtained from local government departments, satellite images or on-site investigation. The boundaries of the area were determined by building locations, functional clusters and road networks. The study firstly divided the whole campus into 13 basic blocks based on road networks, and then randomly combined them based on whether the blocks were adjacent or not, and 28 combined blocks were generated, consequently a total of 41 blocks were obtained. Each block has its own morphology, such as building geometry (height, building density, vertical-to-horizontal area ratio), vegetation, road structure and materials. Figure 5 shows the process of generating blocks from building footprints and road networks.

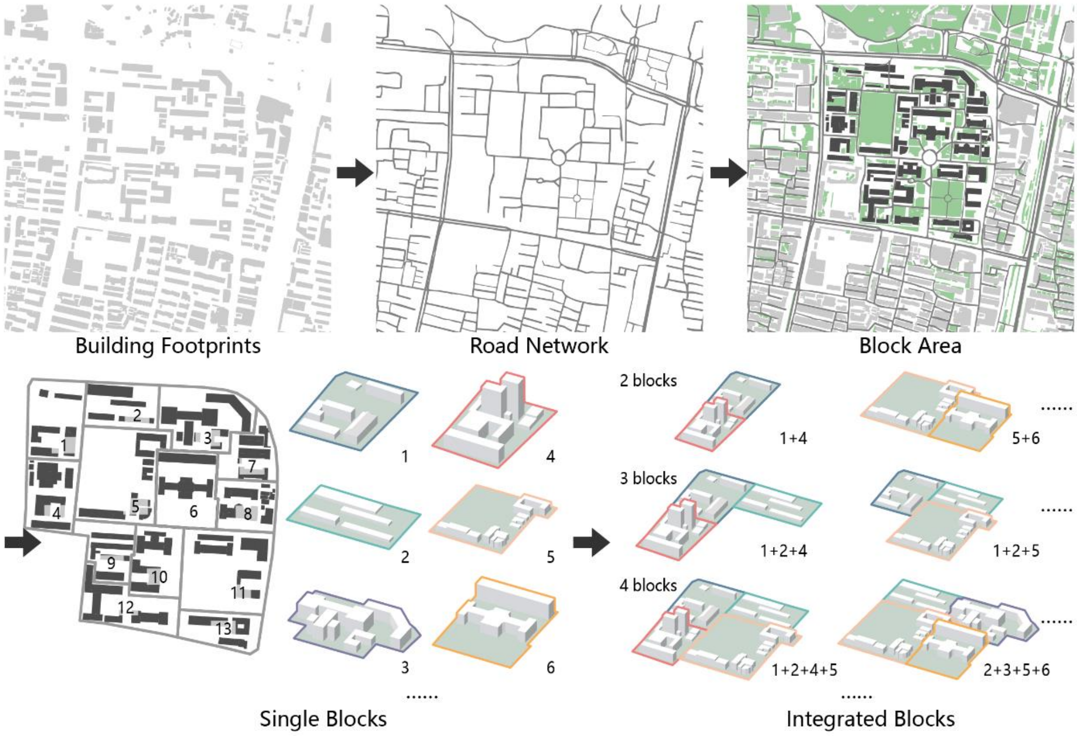

Figure 5: Block generation process based on building footprint and road network

2.4.2 UWG model

After generating the blocks and extracting the morphological parameters of each block, UWG is applied to transform the original weather data. Figure 6 illustrates how the information was exchanged between modules in the UWG model. The UWG can integrate simulation by introducing multiple models, performing synchronization between the models to exchange information on boundaries, allowing larger-scale models to provide boundary information for smaller-scale models. The UWG includes four modules, namely Weather Station Module (WSM), Vertical Diffusion Module (VDM), Target Parcel Boundary Module (TPBM) and Target Parcel Canopy Module (TPCM).

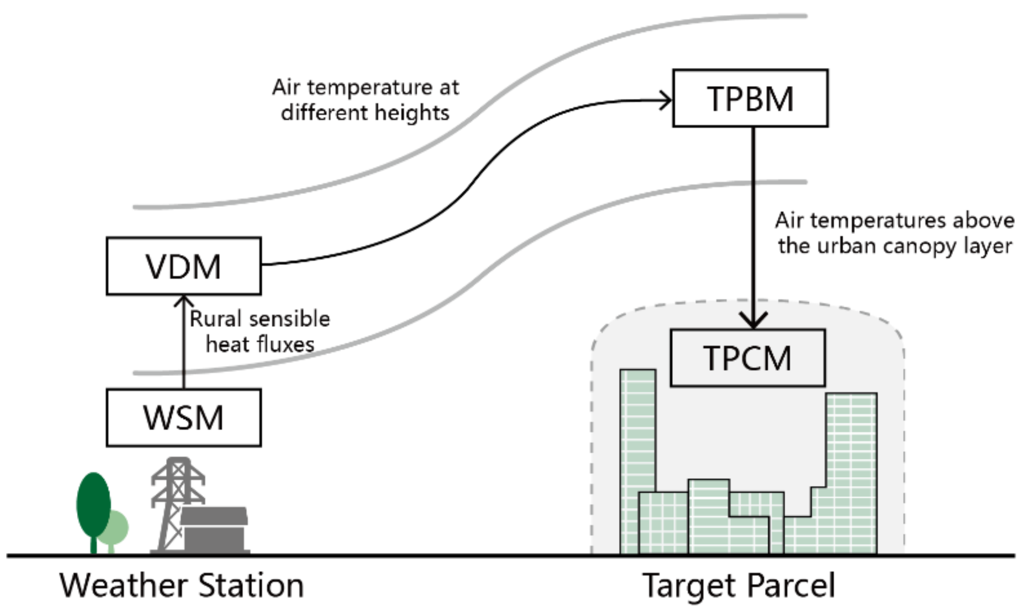

Figure 6: Information exchanged among UWG modules

The WSM is a rural canopy model that contains raw data collected by the meteorological station in the suburban area and calculates sensible heat fluxes. In this study, the data used here was the EPW data and the Nanjing weather station data. The module is based on the energy balance of the soil surface. Equations 1, 2 and 3 define the heat exchange balance in the first layer, each intermediate layer, and the deepest layer, respectively.

$$d_1 \cdot (\rho c)_1 \cdot \frac{\delta T_1}{\delta t} = C_{1,2} \cdot (T_2 - T_1) + Q_{surf} \tag{1}$$

$$d_i \cdot (\rho c)_i \cdot \frac{\delta T_i}{\delta t} = C_{i,i+1} \cdot (T_{i+1} - T_i) + C_{i,i-1} \cdot (T_{i-1} - T_i) \tag{2}$$

$$d_{n-1} \cdot (\rho c)_{n-1} \cdot \frac{\delta T_{n-1}}{\delta t} = C_{n-i,n} \cdot \left(T_{deep} - T_{n-1}\right) \tag{3}$$

where d_i is the depth, m; $(\rho c)_i$ is the volumetric heat capacity, $Jm^{-3}K^{-1}$; T_i is the average temperature of the layer i, K; $C_{i,j}$ is the mean thermal conductance between two layers, $Wm^{-2}K^{-1}$. Q_{surf} is the sum of net radiation, sensible and latent heat fluxes at the surface, Wm^{-2}. T_{deep} is the annual average temperature of weather station, used as boundary condition deep into the ground, K.

The VDM calculates the vertical distribution of air temperature above the weather station, with heat diffusion defined by Equation 4,

$$\frac{\delta\theta(z)}{\delta t} = -\frac{1}{\rho(z)} \cdot \frac{\delta}{\delta z}(\rho(z) \cdot K_d(z) \cdot \frac{\delta\theta(z)}{\delta z}) \quad (4)$$

where θ is the potential air temperature, K; z is the vertical space component, m; ρ is the air density, kgm^{-3}, and K_d is a diffusion coefficient, m^{2}s^{-1}.

The lower boundary condition of Equation 4 is the temperature measured at the weather station, which is usually 2m; the upper boundary condition is the temperature measured at a height of approximately 150m where the potential temperature is uniform and its vertical slope $\frac{\delta\theta(z)}{\delta z}$ equals to 0.

The TPBM calculates the air temperature above the urban canopy layer. The energy balance calculation is performed based on selected control volumes within the defined urban boundary layer, as defined by Equation 5,

$$V_{CV} \cdot \rho \cdot c_v \cdot \frac{d\theta_{urb}}{dt} = H_{urb} + \int u_{ref} \cdot \rho \cdot c_p \cdot (\theta_{ref} - \theta_{urb}) dA_f \quad (5)$$

where V_{CV} is the control volume, m^3; ρ is the air density, kgm^{-3}; c_v and c_p are the specific heat of air at constant volume and constant pressure, respectively, Jkg^{-1}K^{-1}; θ_{urb} and θ_{ref} are the average potential temperature and reference potential temperature of the control volume, respectively, K; H_{urb} is the sensible heat flux at the surface of the control volume, W; u_{ref} is the reference air velocity, ms^{-1}; and A_f is the lateral heat exchange area between the control volume and its surroundings, m^2.

This module distinguishes between nighttime and daytime parcel boundary layers and is driven by the geostrophic wind and the urban breeze circulation. The circulation velocity (u_{circ}) was calculated from the expression given by Hidalgo et al. [46], see Equation 6,

$$u_{circ} = k_w \cdot (\beta \cdot z_i \cdot \frac{H_{tp} - H_{ms}}{\rho \cdot c_p})^{1/3} \quad (6)$$

where k_w is a constant approximating to 1; β is the buoyancy coefficient, ms^{-1}K^{-1}; and H_{tp} and H_{ms} are the sensible heat fluxes from the target parcel and the weather station, respectively, Wm^{-2}.

Based on the morphological parameters within the corresponding target parcel and the results of TPBM calculations, the TPCM will give the adjusted weather data of the target block. The module assumes a good air mixture within the urban canopy. Thus, the energy balance equation of the target parcel is Equation 7,

$$\begin{aligned} Q = {} & T_{road} \cdot h_{cv} \cdot A_{road} + T_{ubl} \cdot A_{road} \cdot u_{ex} \cdot c_p \cdot \rho_{air} + T_{indoor} \cdot A_{win} \cdot U_{win} \\ & + T_{wall} \cdot h_{cv} \cdot A_{wall} + T_{indoor} \cdot A_{roof} \cdot R_{vent} \cdot h_{bld} \cdot c_p \cdot \rho_{air} \\ & + T_{indoor} \cdot A_{roof} \cdot R_{infi} \cdot h_{bld} \cdot c_p \cdot \rho_{air} + \left(A_{roof} + A_{road}\right) \\ & \cdot \left(h_{anthrop} + h_{tree} \cdot \rho_{veg}\right) + A_{roof} \cdot h_{waste} \cdot h_{mix} + A_{win} \\ & \cdot h_{solRec} \cdot (1 - shgc) \end{aligned} \quad (7)$$

where A_{road}, A_{win}, A_{wall} and A_{roof} are the areas of roads, windows, walls and roofs, respectively, m^2; h_{cv} and h_{rd} are convective and radiant heat transfer coefficients, Wm^{-2}K^{-1}; R_{vent} and R_{infi} are the ventilation and infiltration air exchange rates of the building, ms^{-1}; U_{win} is the U-factor of windows, Wm^{-2}K^{-1}; $h_{anthrop}$ and h_{tree} are anthropogenic sensible heat and tree sensible heat, Wm^{-2}K^{-1}.

2.4.3 UBEM configuration

The UBEM simulation was mainly based on a Rhino platform, and the Grasshopper plug-in that comes with Rhino is based on data linking and logical operations to enable visual script editing in the Rhino environment. Among the operators supported by Grasshopper, Ladybug Tools is a collection of free open-source plug-ins which can connect Rhino models to run simulation in EnergyPlus and UWG. Figure 7 shows the input parameters for the UBEM configuration and how these are integrated with the UBEM simulation.

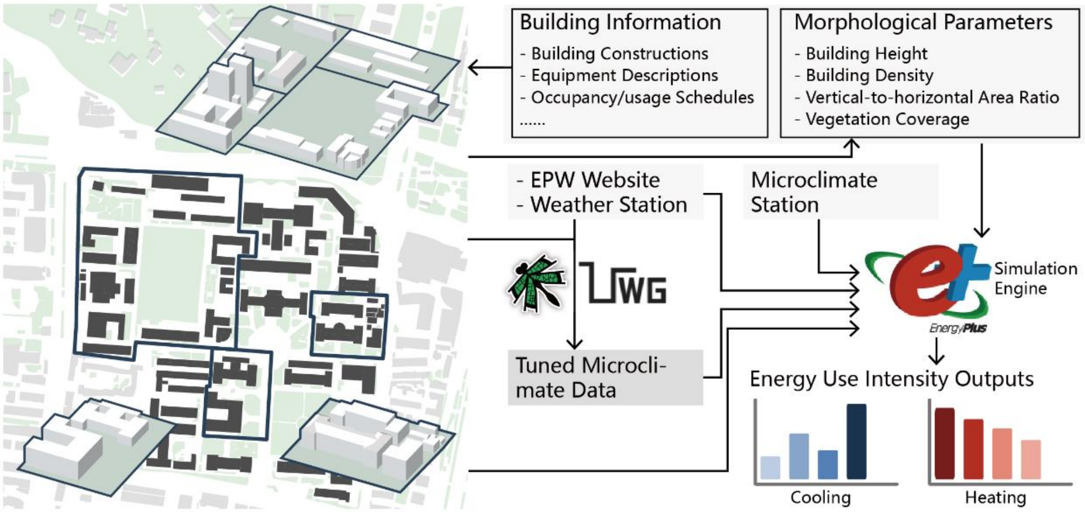

Figure 7: Flowchart of integrating UWG into UBEM

The parameters involved here included weather data, building information and morphological parameters. The EPW data, the Nanjing local climatic data and the microclimate data were taken from different sources and used as initial weather files. At the same time, the first two types of weather data were transformed by UWG to generate block-specific microclimate data. Although building information, such as building construction and equipment descriptions, can be obtained through field observation and experiment, detailed parameters were still lack. This study therefore referred to the *Design Standard for Energy Efficiency of Public Buildings GB 50189-2015* [47] and ASHRAE 90.1 [48] to determine the input parameters based on actual situations. Table 2 displays all the references of input parameters. Then morphological parameters were obtained through on-site survey to establish the building physical model. The input parameters in this study, including load settings, performance characteristics and occupancy schedules, can be referred to our previous work, and the energy simulation results were calibrated through the 20% error requirement and found to be reliable [49].

Table 2: The reference of input parameters besides weather files

Input Parameters	**Reference**
Wall Construction	On-Site Survey
Window Construction	Typical Value of Single Pane
Roof Construction	Typical Value of Honeybee
Floor Construction	Typical Value of Honeybee

Equipment Load Per Area	*Design Standard for Energy Efficiency of Public Buildings GB 50189-2015*
Lighting Density Per Area	*Design Standard for Energy Efficiency of Public Buildings GB 50189-2015*
Air Infiltration Rate	ASHRAE standard 90.1
Number of People Per Area	*Design Standard for Energy Efficiency of Public Buildings GB 50189-2015*
Ventilation Per Person	ASHRAE 90.1

2.5 Performance evaluation index

This study firstly evaluated the temperature differences as reflected by the meteorological data before and after adjustments using root mean square error (RMSE), and then quantified the impact of meteorological data on building energy consumption using mean absolute percentage difference (MAPD) to test the differences between multi-sourced weather files on urban building energy simulation. The calculations of both RMSE and MAPD are shown in Equations 8 and 9, respectively,

$$RMSE = \sqrt{\sum_{i=1}^{n} \frac{(y_i - \widehat{y_i})^2}{n}} \quad (8)$$

$$MAPD = \left(\frac{1}{n}\sum_{i=1}^{n} \frac{|y_i - \widehat{y_i}|}{\widehat{y_i}}\right) * 100\% \quad (9)$$

3. Results

3.1 Results of raw data of multi-sourced microclimate

Figure 8 (above) firstly compares the urban climatic conditions in Nanjing, the monthly average temperatures from multi-sourced meteorological data from three sources. Nanjing has a humid north subtropical climate with four distinct seasons, hot summer and cold winter, with a significant temperature difference between winter and summer. From the overall trend, the temperature trends of Nanjing weather station (WS) and microclimate station in SEU (SEU) are consistent, while EPW and SEU show opposite temperature change trend during June to August. The reason for this difference is inferred to be that the climatic condition of Nanjing in 2020 has some deviation from the meteorological data of 1971-2003 in the EPW file, and climatic condition is inherently random. From the absolute error values of temperature, the maximum absolute error between WS and SEU is 1.96°C, and the mean absolute difference maintains at 1.56°C, while they are 4.83°C and 2.68°C between EPW and SEU, respectively.

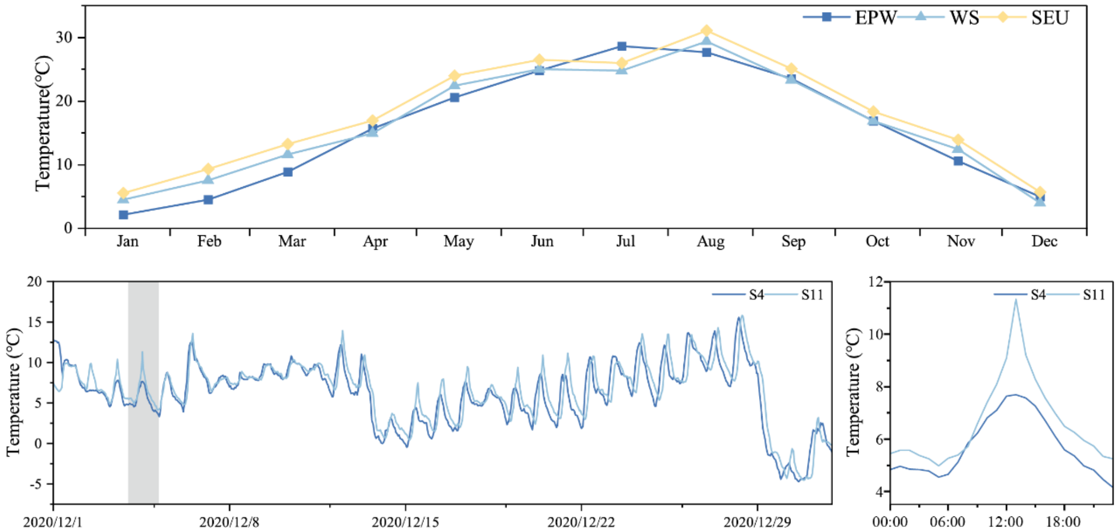

Figure 8: The monthly average temperatures from multi-sourced weather data (above) and hourly air temperature at stationary Site 4 and 11 in December 2020 (left below) and temperature in 4th December 2020 (right below)

Figure 8 (below) shows the hourly temperature results of selected example of two stationary points in December 2020. The temperature values on 1st December, has large deviations, which are excluded as instrument operation errors to avoid interference with the analysis at the beginning of experiment. Subsequently, the temperature showed periodic changes and cooled down significantly twice. Overall, the temperature trends of the two points are very similar, but they still have differences even though both measurement points are in the same campus. The average absolute difference at S4 and S11 is basically within 1°C where the temperature value of S4 is generally lower than S11.This might be S4 is in the inner courtyard enclosed by the teaching buildings blocking solar radiation, while S11 is in the western facade of the teaching building, although there are tall sycamore trees around, but leaves fall off in winter, the effect of blocking solar radiation is weakened.

3.2 Results of Transformed Microclimate

The next is the generated 41 urban blocks according to the Subsection 2.4.1, and the morphological parameters within each block were calculated. Figure 9 presents five generated urban blocks. The four morphological parameters extracted refer to the simulation components of UWG, namely building height (h_{bld}), building density (ρ_{bld}), vertical-to-horizontal area ratio (VH) and vegetation coverage (ρ_{veg}). Overall, h_{bld} and ρ_{bld} are closer within different blocks around 16m and 25%, respectively; VH shows a certain gap in the range of 66% to 86%; ρ_{veg} varied widely among different blocks, and the ρ_{veg} of the whole study area was 32%.

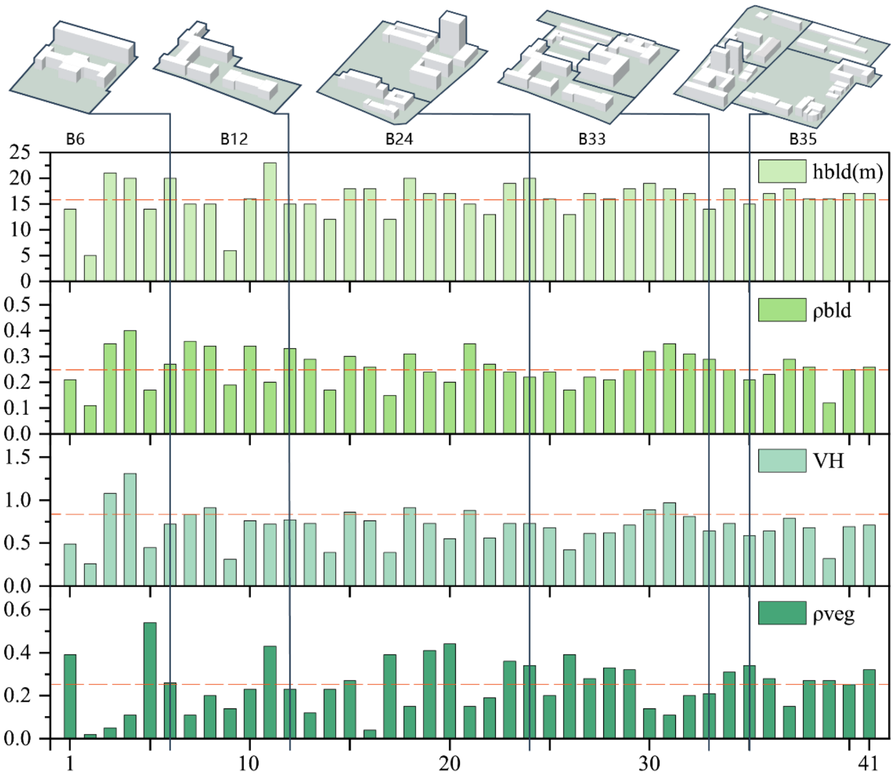

Figure 9: Morphological parameters of blocks (x-axis is the serial number of blocks)

The transformed microclimate weather files specific to each block were obtained from EPW and Nanjing weather station by UWG. The summer solstice and winter solstice were selected as typical day samples to analyze the temperature discrepancy of different weather files in these two days (Figure 10). In the seasonal view, the temperature difference on the summer solstice is small and the average absolute difference of temperature between the weather files before (EPW, WS) and after (EPW-UWG, WS-UWG) and microclimate station (SEU) is basically maintained at 1°C, while the difference on winter solstice is larger, exceeding 3°C.

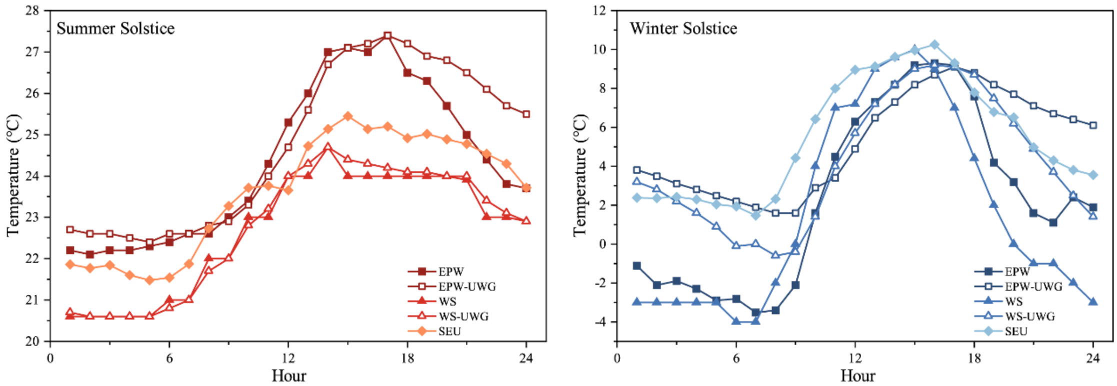

Figure 10: Hourly average temperature on the summer and winter solstice

Eight typical blocks were selected as samples among the 41 blocks, 4 of which were initial blocks and the remaining 4 were combined ones composed of initial blocks, and the transformed EPW and WS within each block were compared with the stationary microclimate points located in each block (Figure 11). Among these 16 points used for the analysis, there are large differences between the measured temperature and it in the transformed weather files at some of the stationary point due to experimental errors, but the transformed weather files from Nanjing weather station (WS-UWG) are undoubtedly more consistent with the microclimate experiment in terms of the overall temperature trends.

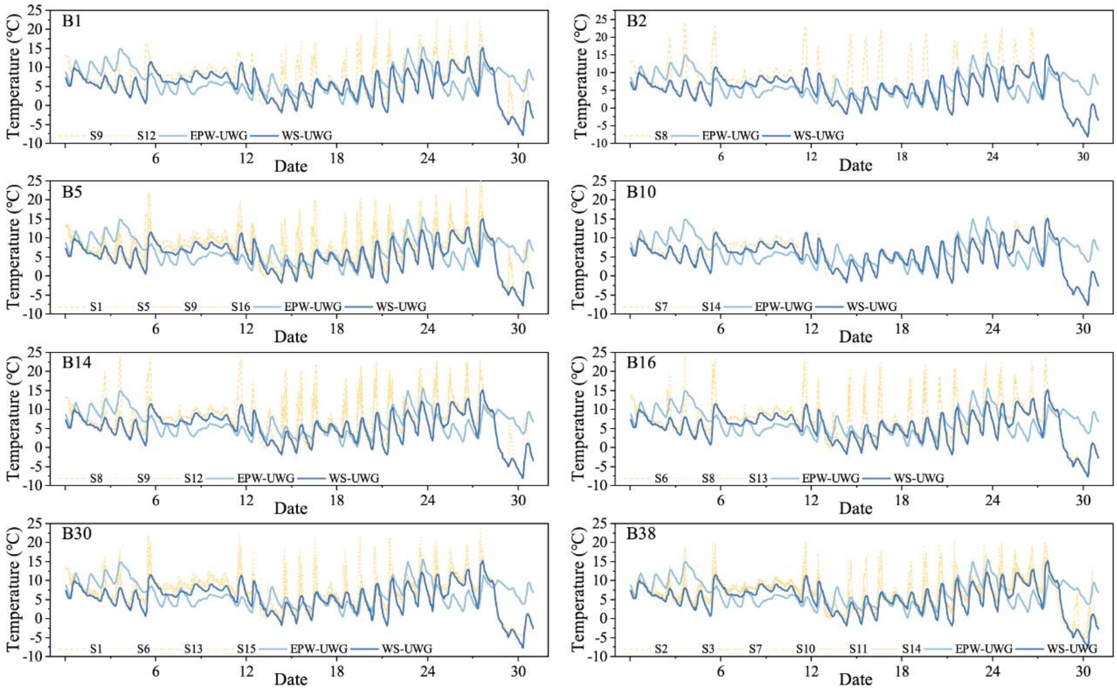

Figure 11: Temperatures of microclimate experimental sites and transformed

microclimate files in eight blocks

Figure 12 shows the analysis results of first two pairs and in Figure 12a, within all the blocks, the RMSE of temperature differences between the transformed microclimate files from Nanjing weather station (WS-UWG) and it from stationary points (Si) is smaller. The average temperature differences between the transformed microclimate files from EPW (EPW-UWG), WS-UWG and Si are 4.5°C and 2.4°C, respectively. The second pair is set up with a scenario where there are no distributed sensors in the study area, but there is a fixed more accurate microclimate station. Figure 12b illustrates the comparisons between transformed weather files between microclimate station, where the results are consistent with the first scenario. The transformed microclimate files from Nanjing weather station perform better, while the average temperature differences in this scenario is 4.1°C and 1.2°C, respectively. In the first two pairs, RMSE of the transformed weather files show a slight difference between blocks when compared with the weather data from microclimate stations. However, when compared with the data from distributed sensors in microclimate experiment, the fluctuation of RMSE varies greatly in different blocks. The change of RMSE is consistent with that of VH and ρ_{veg} in block morphological parameters, while the correlation with h_{bld} and ρ_{bld} is not strong.

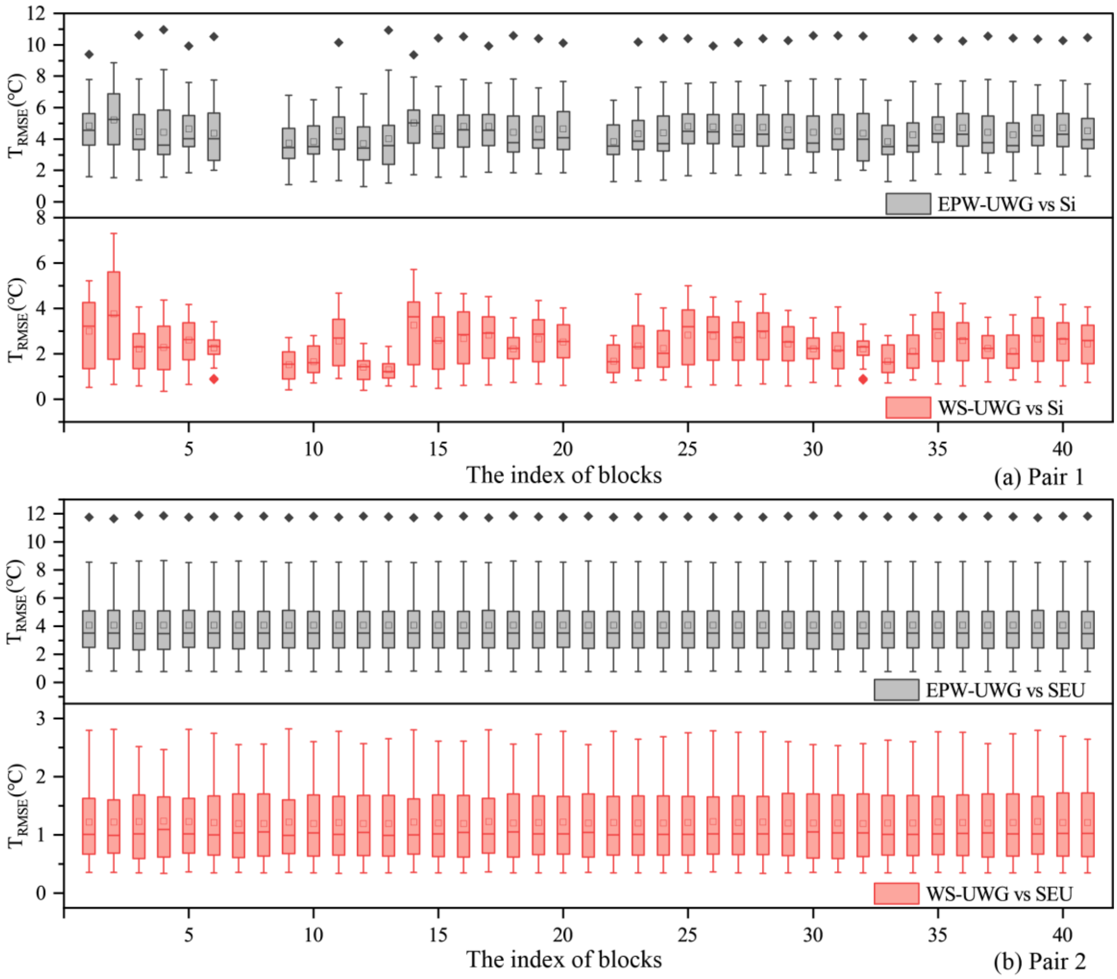

Figure 12: The RMSE of temperature comparison between the first two pairs

The third and fourth pairs are based on the premise that the impact of urban morphology is not considered, and then this study compared the differences between raw EPW, WS and temperature from 16 stationary points (Si), respectively in December. Figure 13a presents that EPW and WS each is closer to the actual monitored values over a period of time and WS still outperforms. The average temperature differences between EPW, WS and weather files from Si are 4.9°C and 3.3°C, respectively. The comparison results between EPW, WS and SEU in Figure 13b imply the same conclusion, while the average temperature differences in this scenario is 4.3°C and 2.1°C, respectively. Meanwhile, comparing the raw weather files with the transformed microclimate files in each block, Figure 13c shows that the temperature adjustment values are closer, and the average temperature difference between the weather files before and after adjustment from EPW and Nanjing weather station is 2.2°C and 2.0°C, respectively.

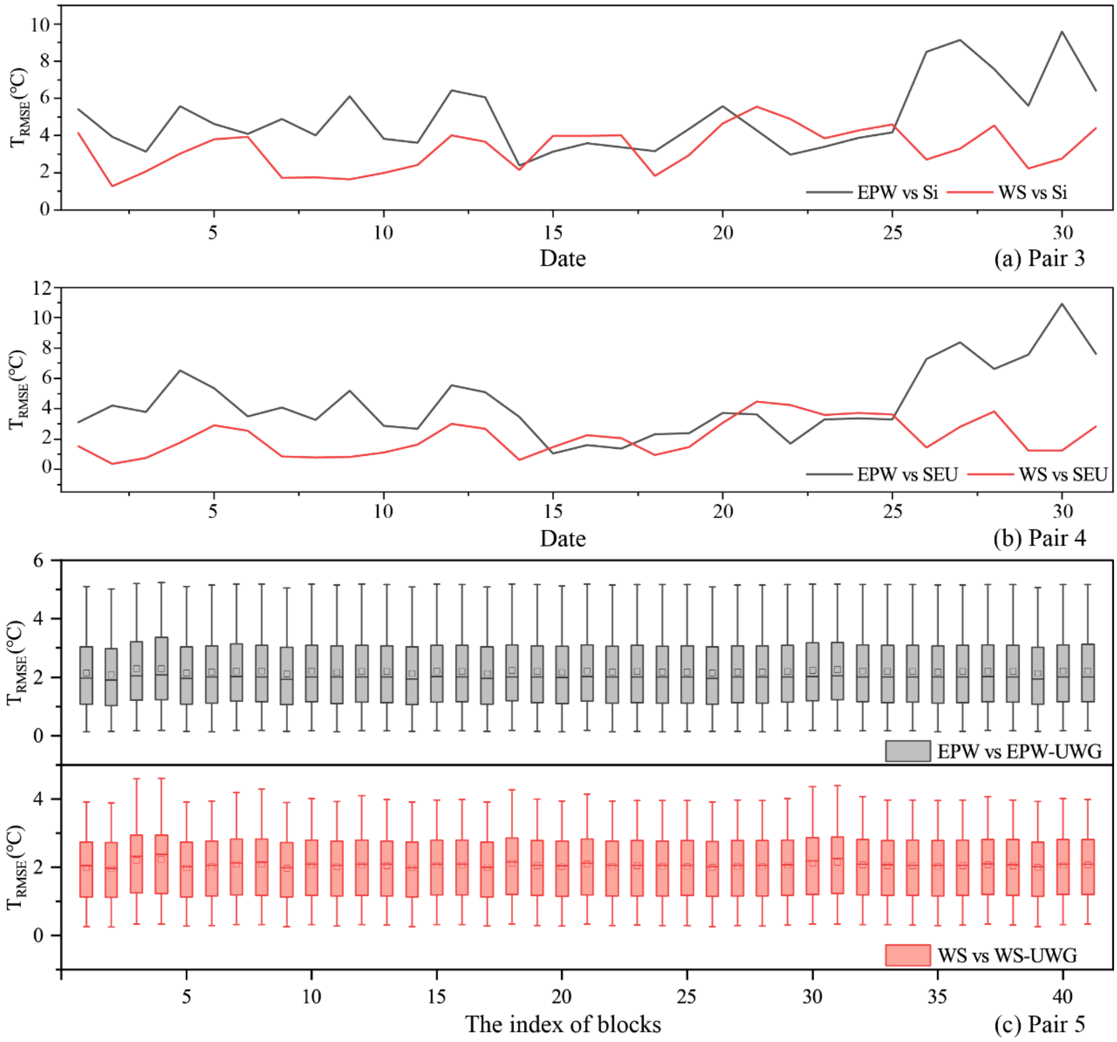

Figure 13: The RMSE of temperature comparison between the last three pairs

Figure 14 is obtained by summarizing the analysis results of the above-mentioned five pairs. Based on the comparison of the first four pairs, it can be clearly concluded that WS performs better than EPW with respect to RMSE of temperature, whether it is the original weather data or the transformed microclimate files. Official weather station of the city where the research is located has a higher priority than EPW when it comes to obtaining weather files for building energy consumption simulation. In addition, comparing pair 1 and 2 with pair 3 and 4 respectively, the results reveal that the transformed microclimate files narrow the gap between the original weather data and the actual measured values, which proves the necessity of considering urban morphology in the process of energy consumption simulation. Meanwhile, although the average temperature adjustments values for EPW and Nanjing weather station are similar, the reduction in the difference between before and after the adjustment and the actual measured values for Nanjing weather station is significantly larger than that for EPW.

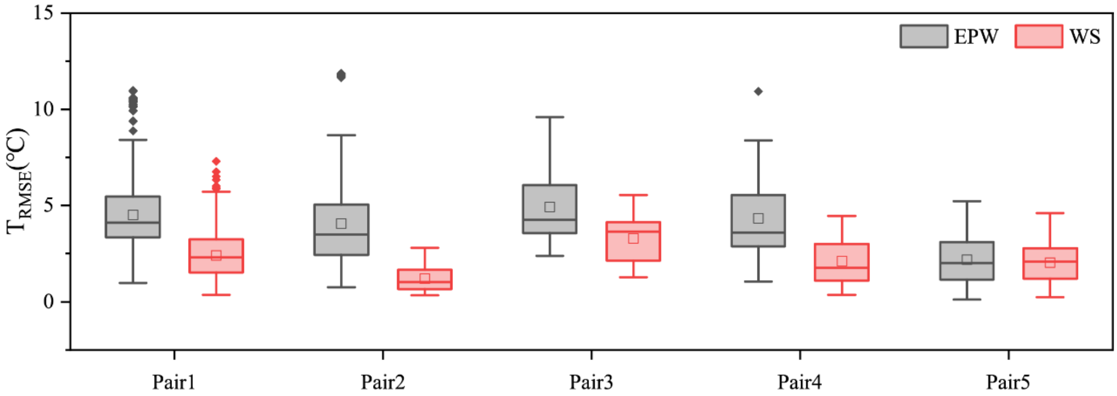

Figure 14: Aggregated RMSE of temperature comparison results

Table 3: Average temperature difference for different pairs' comparison

		Avg. T difference (°C)
Pair 1	EPW-UWG vs Si	4.5
	WS-UWG vs Si	2.4
Pair 2	EPW-UWG vs SEU	4.1
	WS-UWG vs SEU	1.2
Pair 3	EPW vs Si	4.9
	WS vs Si	3.3
Pair 4	EPW vs SEU	4.3
	WS vs SEU	2.1
Pair 5	EPW vs EPW-UWG	2.2
	WS vs WS-UWG	2.1

3.3 Results of Energy Simulation Comparison

To further analyze the influence of weather files on the energy consumption of urban buildings, the weather datasets mentioned above were used as input to simulate the energy consumption of the 41 blocks. This study uses EnergyPlus to calculate the monthly and annual cooling and heating energy consumption of buildings, and then the simulation results use energy use intensity (EUI) as an indicator.

Figure 15 shows the annual EUIs for cooling and heating of buildings in 41 blocks.

Since the building types in the study area are mostly office and teaching buildings, the EUIs for cooling and heating in most of the buildings within the blocks are similar under the same weather file, with the mean annual EUI simulation results for all blocks under SEU being 9.2 kWh/m2/year and 14.6 kWh/m2/year, respectively. Table 4 shows the MAPD of the EUI of buildings in all blocks before and after adjustment of EPW and WS compared with SEU. The results obtained from EPW are closer to those obtained from SEU than those from WS for the cooling EUI, with the mean MAPD of 13.1% and 32.4%, respectively. This is related to the randomness of the Nanjing weather in 2020, where the monthly average temperature of Nanjing for the three months from June to August in EPW is 27.0°C, and the average temperature of WS and SEU are each 26.4°C and 27.8°C. On the other hand, the heating EUI calculated by EPW achieves a mean MAPD of 116.3% when compared to that of SEU, while the mean MAPD of WS is 27.2%. The significant decrease in heating EUI indicates an increasing trend in winter UHI effects when comparing the temperature of Nanjing in 2020 to the weather data collected in EPW after nearly 20 years.

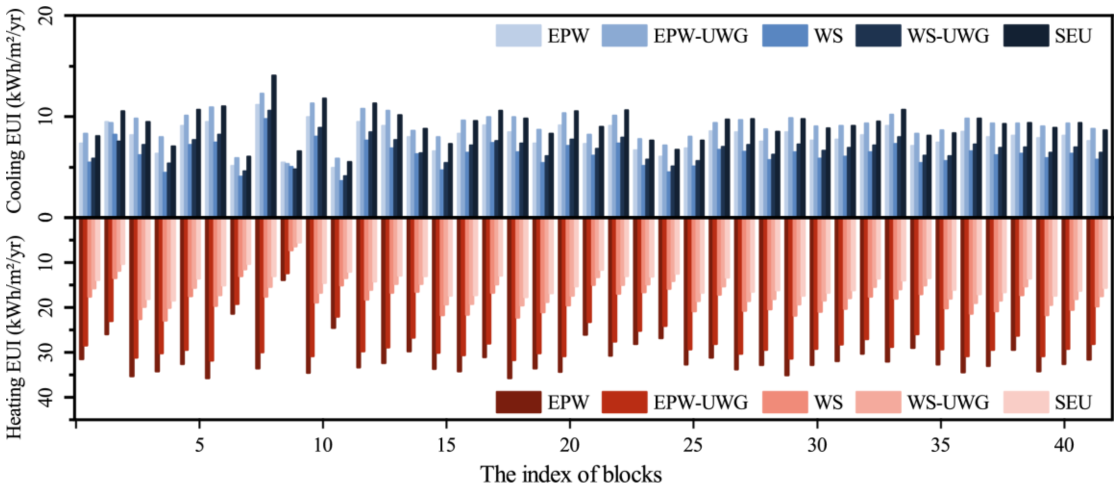

Figure 15: Total annual cooling and heating EUI calculated for all blocks after applying different weather files

Table 4: Mean absolute percentage difference for EUI using different weather data

	Mean absolute percentage difference (%)					
	Cooling		Heating		Total	
Weather data	Mean	Standard Deviation	Mean	Standard Deviation	Mean	Standard Deviation

EPW vs SEU	13.1	2.5	116.3	19.3	65.1	5.6
EPW-UWG vs SEU	4.1	4.0	93.6	17.5	55.9	5.6
WS vs SEU	32.4	2.6	27.2	2.3	4.1	1.4
WS-UWG vs SEU	25.8	1.3	12.7	1.9	2.3	1.5

Figure 16 illustrates the monthly cooling and heating EUI of the buildings throughout the study area. The influence of the transformed microclimate file on building EUI is shown as an increase in cooling load in summer and a decrease in heating load in winter. Comparing the monthly results from different sets of weather data with the results of SEU, the cooling EUIs calculated by SEU are basically the largest, and the heating EUIs calculated by SEU are the smallest. The monthly average temperature of Nanjing in July in EPW is 28.6°C, while that of SEU is 26.0°C, and the cooling temperature setpoint in the energy simulation is 30°C. The duration of July temperature above 30°C hours in EPW and SEU is 283h and 73h, respectively, thus EPW and EPW-UWG both show an unusually high cooling load. Overall, using the results obtained from SEU as a benchmark, EPW performs better than WS in cooling, while WS performs better in heating. Moreover, the transformed microclimate files contribute to the accuracy of the simulation results regardless of cooling or heating, making the results closer to those of SEU.

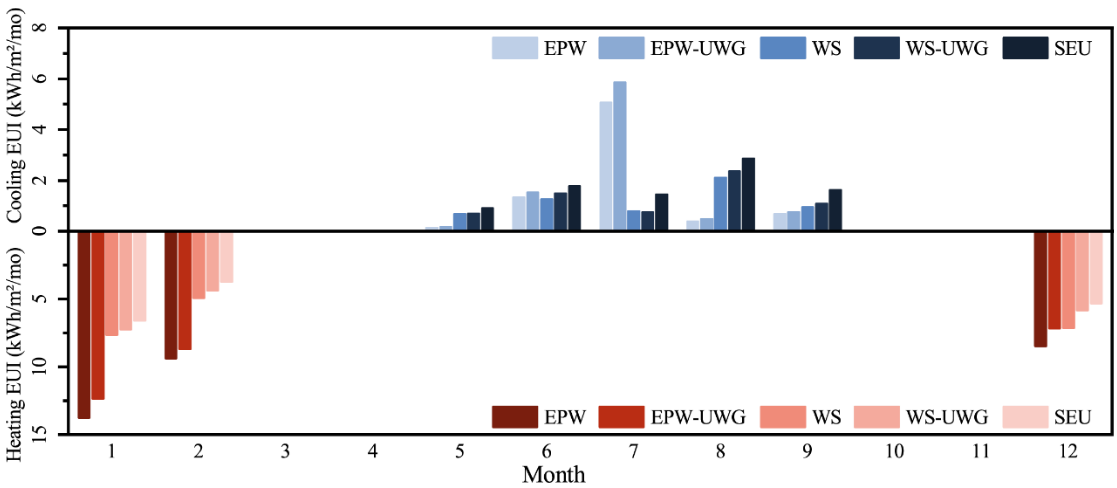

Figure 16: Monthly cooling and heating EUI calculated for the entire campus using different weather files

4. Discussion

To clarify the priority of weather files, this study conducted a comparison of multi-sourced climate datasets. The results show that the RMSE of temperature differences from Nanjing weather station is smaller than that from EPW when comparing urban microclimate, respectively. While the weather files transformed by UWG that considers urban morphology are closer to the stationary points in the field. The results of the simulated EUI show no significant difference between impact of weather files from EPW and Nanjing weather station. The indisputable point is that the transformed EPW and weather station files both improve the accuracy of energy simulation. Although the suburban weather stations better reflect the meteorological conditions in urban areas than EPW, the latter still performs competitively in estimating cooling load as a consolidator of data from previous years. According to the empirical results of this study, when the on-site weather data of the exact location in urban context cannot be obtained, the use of weather files from suburban weather stations and transforming them into microclimate in the urban contexts through simulation software can be preferred. However, in this case, the bias that this choice will have on the energy simulation should also be clarified, which is about 4.1% and 2.3% in this study. The bias from EPW and transformed EPW have an average MAPD of 65.1% and 55.9%.

This study might have those implications. As known, UBEM studies usually require computation sources, especially for larger spatial scales. Therefore, most studies would like to create building prototypes that simplify the morphological characteristics of urban buildings, and this inevitably causes uncertainties in the simulation results since urban morphology has direct and important impacts on energy simulation. This study relies on urban spatial information such as road networks, building footprints and green spaces, which are readily available through the popularization of geographic information services and remote sensing imagery, to divide and combine randomly different urban blocks [50]. Thus, the methodology used in this study is replicable and scalable and can be replicated in different study areas to enhance the findings of this study. On the one hand, urban morphological parameters are extracted and energy consumption simulations are performed by each block, to reduce the computational cost and improves the robustness of results, and on the other hand, the uncertainty inherent in the results is reduced by increasing the randomness of the simulation samples [51,52]. From these two points, this method can be further extended and adopted in larger-scale UBEM studies and it will provide a reference for the researches on the correlation between urban morphology and building energy consumption. Next, in the subsequent application scenarios of the research results, for urban planners, the impact of urban morphology in the built environment on urban heat environment and energy performance can be used as a basis for the retention or demolition of buildings in urban renewal or design.

This study still has some limitations. First, this research uses the UWG model for urban microclimate simulation, but UWG does not have a component of water bodies, which has positive benefits for mitigating UHI and improving urban microclimate. While in the center of the study area, there is a fountain, which might have unavoidable impact on the simulation results of UWG. Therefore, it is necessary to further include such impact from urban blue space, by integrating ENVI-met or other tools. Secondly, there is a lack of further analysis of the meteorological data from the 16 points involved. If it is difficult to install a stable microclimate station, the impacts including the location, validation of a specific monitoring, and how to represent a larger-scale area should be investigated in the future. Lastly, only the microclimate station data from 2020 and the stationary measurement from December 2020 were used in the study. In future work, a larger time span and large-scale microclimate should be carried out.

5. Conclusion

For UBEM, one major parameter is weather data, and weather data collected from different sources may impact the predicted energy consumption from buildings at urban level. To gain a deep understanding on this impact and guide the weather data selection in future studies, this study therefore has considered multi-sourced weather data, namely, EnergyPlus weather, the weather data from Nanjing weather station, the weather data from one microclimate station in SEU and sixteen stationary measurement points in SEU. The transforming of both EPW and WS files to urban context was achieved by the urban weather generator (UWG) tool. To improve simulation accuracy, urban morphological parameters were integrated using a random combination of block division. The main findings from this study include:

- The suburban weather stations reflect urban microclimate better than EPW with more accurately predicted building energy consumption. The results of temperature comparison showed that the RMSE of temperature differences between EPW, the weather files from WS and the microclimate station in SEU were 4.3°C and 2.1°C, respectively. The simulation results for the total energy use intensity using WS and EPW had a MAPD of 4.1% and 65.1%, respectively.

- After adjustment, the gap between simulation results and actual situations was reduced for weather data. The results of temperature comparison showed that the RMSE of temperature difference between the weather files from WS, after adjustment, and that from the microclimate station in SEU was reduced by 0.9°C, and for EPW, it was reduced by 0.2°C.

- This change of weather data was also revealed for building energy consumption simulation. The results of EUI comparison showed a 6.6% reduction in MAPD for the heating EUI calculated using the transformed WS file compared to that calculated using the SEU file, and a 14.2% reduction in MAPD for the cooling EUI. For the transformed EPW file, the MAPDs of the cooling and heating EUIs were reduced by 9% and 22.7%, respectively.

Overall, the suburban weather stations perform better than EPW and the operation of transforming weather data is necessary, but the site-specific weather files are of utmost importance for the reliability of building energy consumption assessment. This study provides important reference for the acquisition and selection of weather files in future UBEM studies, to order to provide reliable simulation results for urban energy system planning, or energy simulation of single buildings in urban context. Also, the results of this study can also enable architects, urban planners, grid planning engineers and relevant policy makers to make more reasonable decisions when identifying the role of urban morphology.

Acknowledgement

The work described in this paper was sponsored by National Science and Foundation of China (#52208011&51978147) and Postgraduate Research & Practice Innovation Program of Jiangsu Province (SJCX22_0034). Any opinions, findings, conclusions, or recommendations expressed in this paper are those of the authors and do not necessarily reflect the views of those organizations.

References

[1] National Statistical Bureau of the People’s Republic of China, Statistical Bulletin of the People’s Republic of China on National Economic and Social Development in 2022, 2023.

[2] G.A. Gonzalez, Urban sprawl, global warming and the limits of ecological modernisation, Env. Polit. 14 (2005) 344–362. https://doi.org/10.1080/0964410500087558.

[3] Z.A. Rahaman, A. Al Kafy, M. Saha, A.A. Rahim, A.I. Almulhim, S.N. Rahaman, M.A. Fattah, M.T. Rahman, K. S, A. Al Faisal, A. Al Rakib, Assessing the impacts of vegetation cover loss on surface temperature, urban heat island and carbon emission in Penang city, Malaysia, Build. Environ. 222 (2022) 109335. https://doi.org/10.1016/j.buildenv.2022.109335.

[4] X. Zhang, F. Wang, Hybrid input-output analysis for life-cycle energy consumption and carbon emissions of China’s building sector, Build. Environ. 104 (2016) 188–197. https://doi.org/10.1016/j.buildenv.2016.05.018.

[5] T. Hong, Y. Chen, X. Luo, N. Luo, S.H. Lee, Ten questions on urban building energy modeling, Build. Environ. 168 (2020) 106508. https://doi.org/10.1016/j.buildenv.2019.106508.

[6] N. Buckley, G. Mills, C. Reinhart, Z.M. Berzolla, Using urban building energy modelling (UBEM) to support the new European Union’s Green Deal: Case study of Dublin Ireland, Energy Build. 247 (2021). https://doi.org/10.1016/j.enbuild.2021.111115.

[7] C.F. Reinhart, C. Cerezo Davila, Urban building energy modeling - A review of a nascent field, Build. Environ. 97 (2016) 196–202. https://doi.org/10.1016/j.buildenv.2015.12.001.

[8] T. Hong, Y. Chen, S.H. Lee, M.P. Piette, Y. Chen, M.P. Piette, CityBES: A web-based platform to support city-scale building energy efficiency, 5th Int. Urban Comput. Work. San Fr. (2016) 10.

[9] Y.Q. Ang, Z.M. Berzolla, S. Letellier-Duchesne, V. Jusiega, C. Reinhart, UBEM.io: A web-based framework to rapidly generate urban building energy models for carbon reduction technology pathways, Sustain. Cities Soc. 77 (2022) 103534.

[10] J.A. Fonseca, T.A. Nguyen, A. Schlueter, F. Marechal, City Energy Analyst (CEA): Integrated framework for analysis and optimization of building energy systems in neighborhoods and city districts, Energy Build. 113 (2016) 202–226. https://doi.org/10.1016/j.enbuild.2015.11.055.

[11] M. Ferrando, F. Causone, T. Hong, Y. Chen, Urban building energy modeling (UBEM) tools: A state-of-the-art review of bottom-up physics-based approaches, Sustain. Cities Soc. 62 (2020) 102408. https://doi.org/10.1016/j.scs.2020.102408.

[12] C. Cerezo Davila, C.F. Reinhart, J.L. Bemis, Modeling Boston: A workflow for the efficient generation and maintenance of urban building energy models from existing geospatial datasets, Energy. 117 (2016) 237–250.

[13] J. Roth, A. Martin, C. Miller, R.K. Jain, SynCity : Using open data to create a synthetic city of hourly building energy estimates by integrating data-driven and physics-based methods Nomenclature :, 280 (2020).

[14] C. Wang, M. Ferrando, F. Causone, X. Jin, X. Zhou, X. Shi, Data acquisition for urban building energy modeling: A review, Build. Environ. 217 (2022) 109056. https://doi.org/10.1016/J.BUILDENV.2022.109056.

[15] N. Fumo, A review on the basics of building energy estimation, Renew. Sustain. Energy Rev. 31 (2014) 53–60. https://doi.org/10.1016/j.rser.2013.11.040.

[16] G. Murano, D. Dirutigliano, V. Corrado, Improved procedure for the construction of a Typical Meteorological Year for assessing the energy need of a residential building, J. Build. Perform. Simul. 13 (2020) 139–151. https://doi.org/10.1080/19401493.2018.1479774.

[17] R.S. McLeod, C.J. Hopfe, Y. Rezgui, A proposed method for generating high resolution current and future climate data for Passivhaus design, Energy Build. 55 (2012) 481–493. https://doi.org/10.1016/j.enbuild.2012.08.045.

[18] N.B. Grimm, S.H. Faeth, N.E. Golubiewski, C.L. Redman, J. Wu, X. Bai, J.M. Briggs, Global change and the ecology of cities, Science (80-.). 319 (2008) 756–760. https://doi.org/10.1126/science.1150195.

[19] T.R. OKE, The energetic basis of the urban heat island, Q. J. R. Meteorol. Soc. 108 (1982).

[20] C. Guattari, L. Evangelisti, C.A. Balaras, On the assessment of urban heat island phenomenon and its effects on building energy performance: A case study of Rome (Italy), Energy Build. 158 (2018) 605–615. https://doi.org/10.1016/j.enbuild.2017.10.050.

[21] T. Hong, Y. Xu, K. Sun, W. Zhang, X. Luo, B. Hooper, Urban microclimate and its impact on building performance: A case study of San Francisco, Urban Clim. 38 (2021) 100871. https://doi.org/10.1016/J.UCLIM.2021.100871.

[22] J. Hidalgo, V. Masson, A. Baklanov, G. Pigeon, L. Gimeno, Advances in urban climate modeling, Ann. N. Y. Acad. Sci. 1146 (2008) 354–374. https://doi.org/10.1196/annals.1446.015.

[23] R. Yao, Q. Luo, Z. Luo, L. Jiang, Y. Yang, An integrated study of urban microclimates in Chongqing, China: Historical weather data, transverse measurement and numerical simulation, Sustain. Cities Soc. 14 (2015) 187–199. https://doi.org/10.1016/j.scs.2014.09.007.

[24] H. Bherwani, A. Singh, R. Kumar, Assessment methods of urban microclimate and its parameters: A critical review to take the research from lab to land, Urban Clim. 34 (2020) 100690. https://doi.org/10.1016/j.uclim.2020.100690.

[25] M. Santamouris, N. Papanikolaou, I. Koronakis, I. Livada, D. Asimakopoulos, Thermal and air flow characteristics in a deep pedestrian canyon under hot weather conditions, Atmos. Environ. 33 (1999) 4503–4521. https://doi.org/10.1016/S1352-2310(99)00187-9.

[26] M. Shahrestani, R. Yao, Z. Luo, E. Turkbeyler, H. Davies, A field study of urban microclimates in London, Renew. Energy. 73 (2015) 3–9. https://doi.org/10.1016/j.renene.2014.05.061.

[27] J.A. Voogt, T.R. Oke, Thermal remote sensing of urban climates, Remote Sens. Environ. 86 (2003) 370–384. https://doi.org/10.1016/S0034-4257(03)00079-8.

[28] M. Stathopoulou, C. Cartalis, Daytime urban heat islands from Landsat ETM+ and Corine land cover data: An application to major cities in Greece, Sol. Energy. 81 (2007) 358–368. https://doi.org/10.1016/j.solener.2006.06.014.

[29] L. Liu, Y. Zhang, Urban heat island analysis using the landsat TM data and ASTER Data: A case study in Hong Kong, Remote Sens. 3 (2011) 1535–1552. https://doi.org/10.3390/rs3071535.

[30] F. Chen, H. Kusaka, R. Bornstein, J. Ching, C.S.B. Grimmond, S. Grossman-Clarke, T. Loridan, K.W. Manning, A. Martilli, S. Miao, D. Sailor, F.P. Salamanca, H. Taha, M. Tewari, X. Wang, A.A. Wyszogrodzki, C. Zhang, The integrated WRF/urban modelling system: Development, evaluation, and applications to urban environmental problems, Int. J. Climatol. 31 (2011) 273–288. https://doi.org/10.1002/joc.2158.

[31] S. Pothiphan, N. Khajohnsaksumeth, B. Wiwatanapataphee, Effects of the wind

speeds on heat transfer in a street canyon with a skytrain station, Adv. Differ. Equations. 2019 (2019). https://doi.org/10.1186/s13662-019-2175-4.

[32] M. Zhang, X. Zhang, S. Guo, X. Xu, J. Chen, W. Wang, Urban micro-climate prediction through long short-term memory network with long-term monitoring for on-site building energy estimation, Sustain. Cities Soc. 74 (2021) 103227.

[33] B. Blocken, LES over RANS in building simulation for outdoor and indoor applications: A foregone conclusion?, 2018. https://doi.org/10.1007/s12273-018-0459-3.

[34] P. Bhiwapurkar, D. Moschandrea, Street geometry and energy conservation of urban buildings in Chicago, Intell. Build. Int. 2 (2010) 233–250. https://doi.org/10.3763/inbi.2010.0047.

[35] J. Zhang, P. Cui, H. Song, Impact of urban morphology on outdoor air temperature and microclimate optimization strategy base on Pareto optimality in Northeast China, Build. Environ. 180 (2020) 107035. https://doi.org/10.1016/j.buildenv.2020.107035.

[36] S. Tsoka, K. Tolika, T. Theodosiou, K. Tsikaloudaki, D. Bikas, A method to account for the urban microclimate on the creation of ‘typical weather year’ datasets for building energy simulation, using stochastically generated data, Energy Build. 165 (2018) 270–283. https://doi.org/10.1016/j.enbuild.2018.01.016.

[37] B. Bueno, L. Norford, J. Hidalgo, G. Pigeon, The urban weather generator, J. Build. Perform. Simul. 6 (2013) 269–281. https://doi.org/10.1080/19401493.2012.718797.

[38] P. Shen, J. Liu, M. Wang, Fast generation of microclimate weather data for building simulation under heat island using map capturing and clustering technique, Sustain. Cities Soc. 71 (2021) 102954. https://doi.org/10.1016/J.SCS.2021.102954.

[39] M. Detommaso, V. Costanzo, F. Nocera, Application of weather data morphing for calibration of urban ENVI-met microclimate models. Results and critical issues, Urban Clim. 38 (2021) 100895. https://doi.org/10.1016/J.UCLIM.2021.100895.

[40] A. Kamal, S.M.H. Abidi, A. Mahfouz, S. Kadam, A. Rahman, I.G. Hassan, L.L. Wang, Impact of urban morphology on urban microclimate and building energy loads, Energy Build. 253 (2021) 111499. https://doi.org/10.1016/J.ENBUILD.2021.111499.

[41] R. Ma, T. Wang, Y. Wang, J. Chen, Tuning urban microclimate: A morpho-patch approach for multi-scale building group energy simulation, Sustain. Cities Soc. 76 (2022) 103516.

[42] P. Eguía Oller, J.M. Alonso Rodríguez, Á. Saavedra González, E. Arce Fariña,

E. Granada Álvarez, Improving the calibration of building simulation with interpolated weather datasets, Renew. Energy. 122 (2018) 608–618. https://doi.org/10.1016/j.renene.2018.01.100.

[43] DOE, Energyplus weather data, (n.d.).

[44] Y. Fu, T. Zhou, I. Lun, F. Khayatian, W. Deng, W. Su, A data-driven approach for window opening predictions in non-air-conditioned buildings, Intell. Build. Int. 14 (2022) 329–345. https://doi.org/10.1080/17508975.2021.1963651.

[45] S. Mishra, S.K. Sharma, Advanced contribution of IoT in agricultural production for the development of smart livestock environments, Internet of Things (Netherlands). 22 (2023) 100724. https://doi.org/10.1016/j.iot.2023.100724.

[46] J. Hidalgo, V. Masson, L. Gimeno, Scaling the daytime urban heat island and urban-breeze circulation, J. Appl. Meteorol. Climatol. 49 (2010) 889–901. https://doi.org/10.1175/2009JAMC2195.1.

[47] M. of H. and U.-R.D. of the P.R. of China, Design standard for energy efficiency of public buildings, (2015).

[48] A. Standard, Energy standard for buildings except low-rise residential buildings, ASHRAE/IESNA Stand. 90 (1999).

[49] Z. Lin, T. Hong, X. Xu, J. Chen, W. Wang, Evaluating energy retrofits of historic buildings in a university campus using an urban building energy model that considers uncertainties, Sustain. Cities Soc. 95 (2023) 104602. https://doi.org/10.1016/j.scs.2023.104602.

[50] S. Vanderhaegen, F. Canters, Mapping urban form and function at city block level using spatial metrics, Landsc. Urban Plan. 167 (2017) 399–409. https://doi.org/10.1016/j.landurbplan.2017.05.023.

[51] Y. Sun, Y. Heo, M. Tan, H. Xie, C.F. Jeff Wu, G. Augenbroe, Uncertainty quantification of microclimate variables in building energy models, J. Build. Perform. Simul. 7 (2014) 17–32. https://doi.org/10.1080/19401493.2012.757368.

[52] E. Prataviera, J. Vivian, G. Lombardo, A. Zarrella, Evaluation of the impact of input uncertainty on urban building energy simulations using uncertainty and sensitivity analysis, Appl. Energy. 311 (2022) 118691. https://doi.org/10.1016/J.APENERGY.2022.118691.